Bifunctional Catalysis by CDP-ribitol Synthase: Convergent Recruitment of Reductase and Cytidylyltransferase Activities in *Haemophilus influenzae* and *Staphylococcus aureus*†

Mark P. Pereira and Eric D. Brown*

Antimicrobial Research Centre, Department of Biochemistry, McMaster University, Hamilton, Ontario L8N 3Z5, Canada

Received June 2, 2004; Revised Manuscript Received July 22, 2004

ABSTRACT: CDP-ribitol synthase catalyzes the formation of CDP-ribitol from ribulose 5-phosphate, NADPH, and CTP. CDP-ribitol is an activated precursor for the synthesis of virulence-associated polysaccharides in the capsule of the Gram-negative pathogen *Haemophilus influenzae* and in the cell walls of Gram-positive pathogens including *Staphylococcus aureus*. We showed previously that CDP-ribitol synthase activity in *H. influenzae* is catalyzed by the bifunctional enzyme Bcs1 in a two-step reaction with reduction preceding cytidylyl transfer [Zolli, M., et al. (2001) *Biochemistry 40*, 5041−5048]. In the work reported here, we predicted a CDP-ribitol synthesis locus in *S. aureus* tandemly arranged as *tarI*, encoding an orthologue of the cytidylyltransferase domain of Bcs1, and *tarJ*, coding for an analogue of the reductase domain of Bcs1. We have shown the formation of a functional CDP-ribitol synthase complex between TarI and TarJ. Steady-state mechanistic studies of the CDP-ribitol synthases TarIJ and Bcs1 revealed that the analogous reductases and orthologous cytidylyltransferases undergo ordered mechanisms. The sequence of substrate binding and product release of the orthologous cytidylyltransferases differed. Steady-state analysis of the reductase and cytidylyltransferase activities of TarIJ indicated a 100-fold difference in the turnover where the primary reductase was rate limiting. Rapid mixing experiments revealed the presence of ∼12 μM ribitol 5-phosphate at steady state, 100-fold lower than the observed K_m for this intermediate. Analysis of the approach to steady state suggested that channeling was not occurring in the coupled enzyme complex and was an unlikely driving force in the convergent recruitment of reductase and cytidylyltransferase activities in the two CDP-ribitol synthases.

Carbohydrate phosphate polymers have been attributed to the virulence of a variety of bacteria. Ribitol 5-phosphate, in particular, is a key building block of virulence-associated polyol phosphates found in the extracellular capsule of the Gram-negative pathogen *Haemophilus influenzae* (*1*) and in the wall teichoic acid of Gram-positive pathogens such as *Staphylococcus aureus* (*2*). The *H. influenzae* capsule is comprised of repeating units of -3-[β-D-ribose-(1,1)-D-ribitol 5-phosphate-] (*3*) whereas ribitol teichoic acids are repeating units of 1,5-linked ribitol 5-phosphate covalently attached to peptidoglycan via a conserved linkage unit (Scheme 1) (*4*, *5*). In both instances, the activated form of ribitol 5-phosphate for polymer production is CDP-ribitol.

We have undertaken an in-depth, comparative study of steady-state kinetic and physical properties of the bifunctional CDP-ribitol synthases from *S. aureus* and *H. influenzae*. These enzymes catalyze the reduction and cytidylyl transfer of ribulose 5-phosphate using NADPH and CTP,[1] respectively, to form CDP-ribitol. In the case of the *H. influenzae* enzyme, Bcs1, ribulose 5-phosphate reductase and ribitol 5-phosphate cytidylyltransferase activities are encompassed in a single polypeptide, presumably the result of a favorable gene fusion event. In work described here, we show that the CDP-ribitol synthase from *S. aureus* is a heterooligomer of TarI and TarJ proteins, encoding cytidylyltransferase and reductase functions, respectively. Especially remarkable is the finding that while the cytidylyltransferase portions of the two CDP-ribitol synthases show orthology, the reductase

Scheme 1: Structure of Poly(ribitol phosphate)−Teichoic Acid Linked to Peptidoglycan in the Gram-Positive Pathogen *S. aureus* (Top) and -3-[β-D-Ribose-(1,1)-D-ribitol 5-phosphate-] Capsular Polymer in the Gram-Negative Pathogen *H. influenzae* (Bottom)

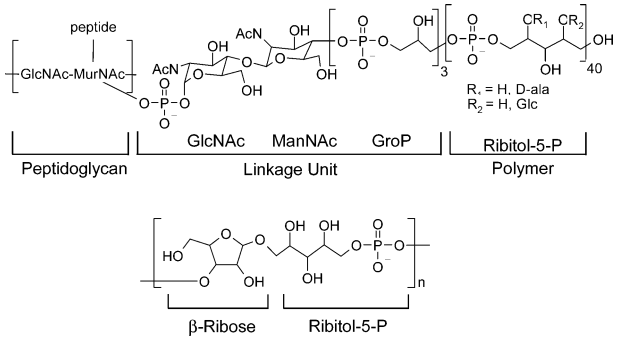

† This work was supported by an operating grant (MOP-15496) from the Canadian Institutes of Health Research.

* To whom correspondence should be addressed. Phone: (905) 525-9140 ext 22392. Fax: (905) 522-9033. E-mail: ebrown@mcmaster.ca.

[1] Abbreviations: HEPES, 4-(2-hydroxyethyl)-1-piperazineethanesulfonic acid; DTT, dithiothreitol; Amp, ampicillin; IPTG, isopropyl β-D-thiogalactopyranoside; $MgCl_2$, magnesium chloride; CTP, cytidine triphosphate; PP_i, pyrophosphate. All phosphorylated carbohydrates are in the D-(+) conformations.

10.1021/bi048866v CCC: $27.50
Published on Web 08/27/2004

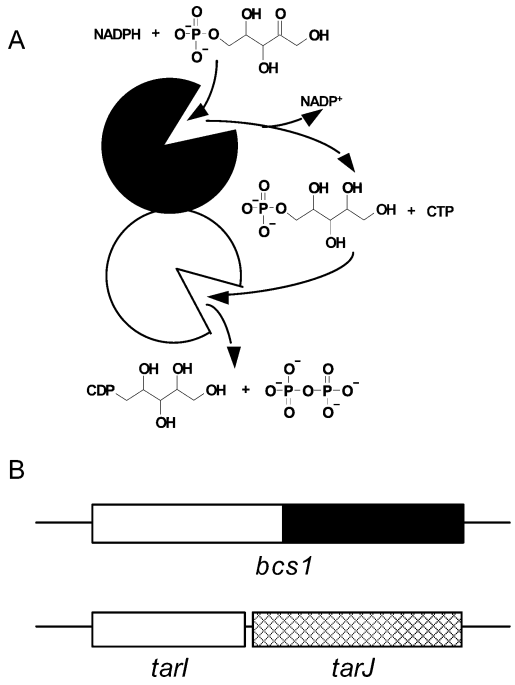

FIGURE 1: Reaction and domain organization of CDP-ribitol synthases from *H. influenzae* and *S. aureus*. (A) A two active site model has previously been proposed for the bifunctional catalysis of Bcs1. Reduction of ribulose 5-phosphate to ribitol 5-phosphate by NADPH precedes nucleotidyl transfer of CTP to form CDP-ribitol (*6*). (B) CDP-ribitol synthase in *H. influenzae* is encoded by a single open reading frame (ORF), *bcs1*, whereas in *S. aureus* we found that this activity is encoded by two separate ORFs, *tarI* and *tarJ*, found tandemly in the genome. The cytidylyltransferase domains encoded by *bcs1* and *tarI* were found to be homologous with 36% sequence identity. However, the reductase domains encoded by *bcs1* and *tarJ* are analogous. The Bcs1 reductase domain belongs to the short-chain dehydrogenase/reductase family (*10*) while TarJ belongs to the alcohol dehydrogenase/reductase family (*11*).

functions are evolutionarily unrelated, analogous components. The bifunctionality of these enzymes raises mechanistic issues that are peculiar to bifunctional enzymes in metabolism. In particular, we are trying to understand the logic behind gene fusion and heterooligomerization of the two activities through careful investigation of the structure and function of these enzymes.

In studies of the bifunctional CDP-ribitol synthase enzyme Bcs1 from *H. influenzae*, we previously established that reduction of ribulose 5-phosphate to the intermediate ribitol 5-phosphate preceded cytidylyl transfer in the formation of CDP-ribitol (Figure 1A). We also ruled out channeling of the intermediate by determining that the two enzymatic steps occurred with release and free diffusion of ribitol 5-phosphate (*6*). With the understanding that the two activities of Bcs1 could be analyzed separately, we have proceeded here to dissect the steady-state kinetic mechanisms of each active site. We have likewise studied the kinetic mechanisms of these activities in the CDP-ribitol synthase from *S. aureus*.

The N-terminal region of Bcs1 encodes a nucleotidyltransferase domain that shows closest homology to 4-diphosphocytidyl-2-*C*-methylerythritol synthetase (IspD/YgbP) and *N*-acetylglucosamine-1-phosphate uridyltransferase (GlmU). These enzymes share a conserved L-X_2-G-X-G-T-X-M-X_4-P-K motif (*7*, *8*) involved in substrate binding and catalysis. Currently, structural data for both GlmU and IspD are available (*8*, *9*); however, the steady-state mechanism of this important class of nucleotidyltransferases has not yet been addressed. In *S. aureus* a predicted 284 amino acid protein, TarI, shares 36% identity to the first 233 amino acids of Bcs1, implicating it as the ribitol 5-phosphate cytidylyltransferase in teichoic acid biosynthesis. Here, we have shown that this protein does indeed catalyze cytidylyl transfer with ribitol 5-phosphate.

The C-terminal region of Bcs1 encodes a reductase domain that is part of the short-chain dehydrogenase/reductase family (*10*). Curiously, a homologue to the reductase portion of Bcs1 could not be found within the *tar* gene cluster which encodes proteins necessary for the synthesis of poly(ribitol phosphate) in *S. aureus*. Instead, we found a 341 amino acid protein encoded in an open reading frame *tarJ*, immediately downstream of *tarI*, that was predicted to be a member of the alcohol dehydrogenase/reductase (ADH) family of enzymes (*11*). Here, we have established a role for this protein, the reduction of ribulose 5-phosphate to ribitol-5-phophate in *S. aureus*.

The CDP-ribitol synthases from *H. influenzae* and *S. aureus* appear to provide an extraordinary example of a Rosetta stone prediction of functional association (*12*−*14*). The Rosetta stone postulate begins with a single polypeptide catalyzing two activities, referred to as a composite protein. The theory hypothesizes that a functional association can be made between two proteins orthologous to the respective domains of the composite protein (*12*, *13*). These proteins, referred to as the component proteins, are predicted to physically associate into a bifunctional complex (*12*). Here, the relationship between the composite protein Bcs1 and the component proteins TarI and TarJ is unconventional as the cytidylyltransferase domains found within TarI and Bcs1 are orthologous, yet the dehydrogenase/reductase domains within TarJ and Bcs1 are analogous (Figure 1B). That is, the reductase domains have the potential to carry out the same reaction, yet have no common ancestral gene. In this work we have unambiguously established that TarI and TarJ enzymes form a complex and have characterized the kinetic mechanistic details of reduction of ribulose 5-phosphate and subsequent cytidylyl transfer to form CDP-ribitol. Similar to Bcs1, our work with TarIJ indicates release and free diffusion of the intermediate ribitol 5-phosphate without channeling between active sites. Nevertheless, we posit that the functional association of reductase and cytidylyltransferase activities in Bcs1 and TarIJ has an indefinable logic that is surely driven by convergent evolutionary forces.

EXPERIMENTAL PROCEDURES

Materials. 4-(2-Hydroxyethyl)-1-piperazineethanesulfonic acid (HEPES), dithiothreitol (DTT), ampicillin (Amp), isopropyl β-D-thiogalactopyranoside (IPTG), and urea were purchased from BioShop Canada Inc. (Burlington, Ontario, Canada). Ammonium sulfate and magnesium chloride ($MgCl_2$) were obtained from BDH Inc. (Toronto, Ontario, Canada). Radiolabeled [5-^{3}H]CTP (22 Ci/mmol, ammonium salt) was purchased from Amersham-Pharmacia (Baie d'Urfé, Quebec, Canada). Sodium pyrophosphate was purchased from Fisher Scientific (Fair Lawn, NJ). Triethylamine (99%) was purchased from Anachemica Canada Inc. (Montreal, Quebec, Canada). The Gateway cloning and expression kit was

purchased from Invitrogen Life Technologies (Carlsbad, CA). Ribitol 5-phosphate was synthesized chemically using ribose 5-phosphate as previously described (*6*). All other chemicals were purchased from Sigma-Aldrich (Oakville, Ontario, Canada).

Construction of the TarIJ Overexpression Plasmid. The genes encoding CDP-ribitol synthase enzymes TarI and TarJ from *S. aureus* were amplified in tandem from genomic DNA using VENT DNA polymerase (NEB Biosciences). Primers were 5′-GGGGACAAGTTTGTACAAAAAAGCAGGCTTAGAAGGAGATAGAACCATGAAATACGCTGGTATTCTAGCT-3′ and 5′-GGGGACCACTTTGTACAAGAAAGCTGGGTCTTACATAATCCATTTTAATACTGT-3′. The PCR-amplified product was cloned into the pDEST14 native expression vector through the use of the Gateway cloning and expression kit, and the insert sequence was confirmed by DNA sequence analysis (MOBIX, McMaster University).

Enzyme Purification. Full-length native TarI and TarJ were coexpressed and copurified from *Escherichia coli* BL21-(DE3) cells transformed with pDEST14-TarIJ grown at 37 °C to an optical density (600 nm) of 0.5 in Luria−Bertani media (4L) supplemented with 50 μg/mL ampicillin. The cells were then induced with 1 mM IPTG and grown for an additional 4 h prior to harvest by centrifugation at 10000*g*. The cells were washed with a 0.85% saline solution, pelleted, and resuspended in 50 mL of lysis buffer (25 mM HEPES, pH 8.0, 1 mM DTT, 0.5 mg of DNase, 0.5 mg of RNase). All subsequent steps were performed at 4 °C. Cells were lysed by passage through a French press at 20000 psi and clarified by centrifugation at 40000*g* for 2 h. Clarified lysate was loaded onto a Q-Sepharose fast-flow column (50 mL; Amersham-Pharmacia, Baie d'Urfé, Quebec, Canada) equilibrated with 25 mM HEPES, pH 8.0, and 1 mM DTT. A gradient of 0−1 M NaCl was applied to the column at a flow rate of 3 mL/min to elute the bound protein. Collected fractions were analyzed by SDS−PAGE and visualized by Coomassie blue staining to identify the proteins of interest. Suitable fractions were pooled and treated with saturated ammonium sulfate to a final concentration of 0.39−1.17 M (10−30%) to precipitate the TarI and TarJ proteins out of solution. The precipitate slurry was centrifuged at 26000*g* for 20 min and decanted. The resulting pellet was resuspended in 5 mL of gel filtration buffer (25 mM HEPES, pH 8.0, 1 mM DTT, 100 mM NaCl) and loaded onto a preequilibrated Superdex 200 gel filtration column (127 mL; Amersham-Pharmacia, Baie d'Urfé, Quebec, Canada). The protein was pooled and stored in aliquots containing 10% glycerol at −80 °C. The concentration of the purified protein was determined by a method described by Gill and von Hippel (*15*). The *H. influenzae* enzyme Bcs1 was overexpressed and purified as previously described (*6*).

Reductase and Cytidylyltransferase Assays. The reductase reactions were assayed continuously by monitoring a decrease in NADPH concentrations using absorbance (absorbance 340 nm, extinction coefficient 6220 M^{-1} cm^{-1}) and fluorescence detection methods (excitation 340 nm, emission 445 nm). Fluorescence measurements were used in situations where low NADPH concentrations required a greater sensitivity. Fluorescence data were collected using a PTI spectrofluorometer (Photon Technologies International, London, Ontario, Canada). Absorbance data were collected using a Spectramax Plus 96-well platereader (Molecular Devices, Sunnyvale, CA). All reductase reactions were performed in triplicate. The cytidylyltransferase reactions were performed in duplicate and monitored in a stopped assay through the conversion of [5-^{3}H]CTP to [5-^{3}H]CDP-ribitol by HPLC as described previously (*16*).

Synthesis of CDP-ribitol. The synthesis of CDP-ribitol was performed enzymatically from the substrates CTP and ribitol 5-phosphate. The following room temperature incubation was prepared: 25 mM HEPES, pH 7.2, 10 mM $MgCl_2$, 1 mM DTT, 0.01% Triton X-100, 20 mM ribitol 5-phosphate, 20 mM CTP, 0.1 unit/μL inorganic pyrophosphatase, and 6.9 μM Bcs1. The progress of the reaction was monitored through absorbance detection at 271 nm using anion-exchange HPLC. The synthesis proceeded to 98% completion and was terminated by removal of protein using an Amicon Ultrafree-MC 5 kDa molecular mass cutoff spin filter. The reaction product was used without any further purification.

Bcs1 and TarIJ Steady-State Kinetic Analysis of Forward Reactions. Initial rate data for Bcs1 and TarIJ were collected at various concentrations of NADPH and ribulose 5-phosphate for the reductase reaction and of CTP and ribitol 5-phosphate for the cytidylyltransferase reaction. The Bcs1 assay mixture for the reductase reaction was composed of 25 mM HEPES, 1 mM DTT, 85 μM CTP, 10 mM $MgCl_2$, 0.01 mg/mL BSA, and 2.26 nM Bcs1. The substrates NADPH and ribulose 5-phosphate were varied from 5 to 60 μM and 50 to 800 μM, respectively. The assay mixture for the cytidylyltransferase reaction was composed of 25 mM HEPES, 1 mM DTT, 85 μM CTP, 10 mM $MgCl_2$, 3 μCi of [5-^{3}H]CTP, 0.01% Triton X-100, and 0.1 nM Bcs1. The substrates CTP and ribitol 5-phosphate were varied from 2.5 to 42.5 μM and 10 to 160 μM, respectively.

The TarIJ assay mixture for the reductase reaction was composed of 25 mM HEPES, 1 mM DTT, 1 μM $ZnCl_2$, 0.01 mg/mL BSA ,and 5 nM TarIJ. The substrates NADPH and ribulose 5-phosphate were varied from 2 to 16 μM and 15 to 240 μM, respectively. The assay mixture for the cytidylyltransferase reaction was composed of 25 mM HEPES, 1 mM DTT, 10 mM $MgCl_2$, 3 μCi of [5-^{3}H]CTP, 0.01% Triton X-100, and 0.5 nM TarIJ. The substrates CTP and ribitol 5-phosphate were varied from 50 to 800 μM and 0.5 to 8.0 mM, respectively.

The data were fit by nonlinear least squares regression to an equation that describes a ternary complex model (eq 1) (*17*) using the Enzyme Kinetics Module 1.1 of Sigmaplot 8.0 (SPSS Inc., Chicago, IL). In the equations, K_a and K_b are the respective Michaelis constants of the substrates while *A* and *B* are their concentrations. K_{ia} is defined to be the dissociation constant for *A* (*17*).

$$v = \frac{V_{max}AB}{K_{ia}K_b + K_aB + K_bA + AB} \quad (1)$$

Bcs1 and TarIJ Product Inhibition Studies. The reductase activities of Bcs1 and TarIJ were monitored in the presence of their product inhibitors $NADP^+$ and ribitol 5-phosphate. Likewise, the cytidylyltransferase activities were monitored in the presence of the product inhibitors pyrophosphate and CDP-ribitol. In these reactions, one substrate was varied in concentrations similar to the initial velocities studies, while the other substrate was fixed at either subsaturating or saturating concentrations. The data from various inhibitor

concentrations were fit by nonlinear least squares regression to models describing competitive (eq 2), noncompetitive (eq 3), uncompetitive (eq 4), or mixed inhibition (eq 5) (*17*) using the Enzyme Kinetics Module 1.1 of Sigmaplot 8.0 (SPSS Inc., Chicago, IL).

$$v = \frac{V_{max}}{1 + (K_m/S)(1 + I/K_i)} \quad (2)$$

$$v = \frac{V_{max}}{(1 + I/K_i)(1 + K_m/S)} \quad (3)$$

$$v = \frac{V_{max}}{1 + I/K_i + K_m/S} \quad (4)$$

$$v = \frac{V_{max}}{(K_m/S)(1 + I/K_i) + (1 + I/(\alpha K_i))} \quad (5)$$

Molecular Weight Determination by Sedimentation Equilibrium. The solution molecular weights of Bcs1 and TarIJ were determined using sedimentation equilibrium analysis performed on the Beckman-Coulter XL-I analytical ultracentrifuge (Palo Alto, CA). Loading concentrations of 3.14, 6.30, and 9.44 μM (corresponding to 0.1, 0.2, and 0.3 A_{280} values, respectively) for Bcs1 and 4.64, 6.97, and 9.29 μM (corresponding to 0.25, 0.38, and 0.5 A_{280} values, respectively) for TarIJ were loaded into a 6-channel epon−charcoal cells with a 1.2 cm path length. Equilibrium of protein concentration gradients was developed for 13−15 h using rotor speeds of 10k−14k rpm for Bcs1 and 11k rpm for TarIJ. The reference solvent was composed of 25 mM HEPES, pH 7.2, and 150 mM NaCl (ρ = 1.007 g/mL) for Bcs1 and 25 mM HEPES, pH 7.2, 200 mM NaCl, 1 mM DTT, and 1 μM $ZnCl_2$ (ρ = 1.009 g/mL) for TarIJ, to which the proteins were dialyzed against. Solvent conditions incorporating 100 μM CTP and 10 mM $MgCl_2$ (ρ = 1.008 g/mL) were investigated for Bcs1 to analyze their impact on oligomer formation. The collected absorbance data (A_{280}) were analyzed using the Beckman-Coulter Optima XL-I Analytical Ultracentrifuge Origin Data Analysis Package (version 60-4) along with Microcoal Origin 6.0. Partial specific volumes (0.737 mL/g for Bcs1 and 0.735 mL/g for TarIJ) and solvent density were calculated using the public domain SEDNTERP program developed by Hayes, Laue, and Philo (http://www.rasmb.bbri.org/). The gradients were fit to a self-association model with a K_d equal to the inverse of $K_{a(conc)}$ calculated using eq 6 (*18*). The molar extinction coefficient ϵ was calculated to be 31770 cm^{-1} M^{-1} for Bcs1 and 53840 cm^{-1} M^{-1} for TarIJ, l is the cell path length of 1.2 cm, n is the order of oligomer formation, and $K_{a(abs)}$ is the absorbance association coefficient determined by nonlinear regression to the proposed model using the analysis software described above. The monomer molecular masses of Bcs1 and TarIJ were 53190 and 65105 Da, respectively, calculated from amino acid sequences. The monomer molecular mass of TarIJ was calculated to be the sum of TarI and TarJ individual monomer molecular masses.

$$K_{a(conc)} = K_{a(abs)} \frac{(\epsilon l)^{n-1}}{n} \quad (6)$$

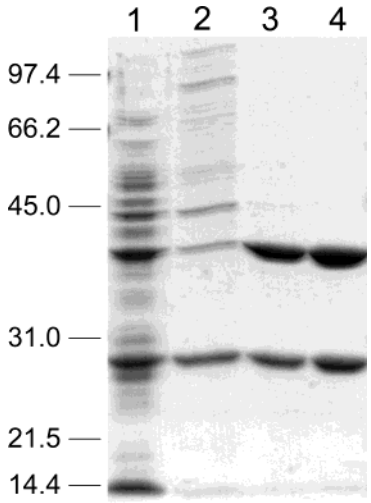

FIGURE 2: Purification of recombinant TarI and TarJ. An SDS−polyacrylamide gel (12% acrylamide w/v) stained with Coomassie blue was used at each step to analyze the sample purity. Shown are clarified cell lysate (50 μg, lane 1), Q-Sepharose anion-exchange pool (20 μg, lane 2), 10−30% ammonium sulfate cut (20 μg, lane 3), and Superdex 200 gel filtration pool (20 μg, lane 4). Prior to electrophoresis, proteins were denatured by boiling in Laemmli buffer (*31*) containing 5% 2-mercaptoethanol. TarI and TarJ copurified in apparent stoichiometry with molecular masses of roughly 26 and 41 kDa, respectively.

RESULTS

Overexpression and Purification of TarIJ. We first attempted to overproduce TarI and TarJ individually from their respective genes using the T7 expression system described herein but found no obvious protein overexpression on analysis of either of these clones using SDS−PAGE with Coomassie brilliant blue detection (data not shown). We turned instead to a single T7 expression construct (pDEST14-TarIJ) that contained these genes in tandem just as they are present on the *S. aureus* chromosome. Figure 2 shows SDS−PAGE analysis of the cell lysate and three purification steps where species with apparent molecular masses of 26 and 41 kDa, corresponding to those of TarI (26.7 kDa) and TarJ (38.5 kDa), respectively, copurified in roughly equimolar ratios. The notion that these proteins copurified as a complex was further tested with another overexpression construct that placed a hexahistidine tag at the amino terminus of TarI in the tandem overexpression system. Purification of the hexahistidine-tagged TarI using nickel affinity chromatography resulted in copurification of apparently equimolar TarJ (data not shown).

Molecular Mass Determination of Bcs1 and TarIJ. To determine the solution molecular mass of Bcs1 and TarIJ, we used analytical sedimentation techniques. Sedimentation equilibrium data collected for Bcs1 at multiple rotor speeds were best fit with a monomer−dimer association model with a dissociation constant of 1.26 μM and a homodimer of 106.4 kDa (Table 1 and Supporting Information Figure 1). We noted previously that the combination of $MgCl_2$ and CTP appeared to stabilize purified preparations of Bcs1 in our assay systems (*6*). We therefore also collected sedimentation equilibrium data in the presence of $MgCl_2$ (10 mM) and CTP (100 μM). In these conditions (Bcs1 ranged in concentration from 3.8 to 11 μM) the homodimer predominates such that

Table 1: Oligomeric State of CDP-ribitol Synthase

	Bcs1	TarIJ
Stokes radii[a]		3.99 nm
$s_{20,w}$[b]		7.26 S
monomer MW[c]	53190 Da	65105 Da
oligomer formation[d]	dimer	dimer (I_2J_2)
K_d[d]	1.26 μM	0.76 μM
$K_{d,+CTP}$[e]	single species dimer	
calculated MW[f]		129 kDa
oligomer MW[g]	106380 Da	130210 Da

[a] Determined from gel filtration chromatography. See Supporting Information Figure 2 (inset). [b] Determined from sedimentation velocity studies. See Supporting Information Figure 2. [c] Calculated from amino acid composition; in the case of TarIJ the value is the sum of the individual molecular masses of TarI and TarJ. [d] Determined from sedimentation equilibrium experiments. See Supporting Information Figures 1A and 3. [e] Determined from sedimentation equilibrium experiments performed in the presence of 100 μM CTP and 10 mM $MgCl_2$. See Supporting Information Figure 1B. [f] Calculated from eq 7 using gel filtration and sedimentation velocity data. [g] Calculated from the amino acid composition of the proposed oligomer formed.

a single species of 106.4 kDa was predicted by the analysis (Table 1).

Analysis of the solution molecular mass of TarIJ was complicated by the fact that a number of models are possible for the formation of oligomers including the two species. SDS−PAGE analysis with Coomassie brilliant blue staining of purified protein revealed roughly stoichiometric amounts of TarI and TarJ. Sedimentation velocity and gel filtration experiments on purified protein revealed a sedimentation constant of 7.26 S and a Stokes radius of 3.99 nm, respectively. The anhydrous molecular mass (m) of the TarIJ complex was determined to be 129 kDa (Table 1, Supporting Information Figure 2) using the relationship described in eq 7 where N_A is Avogadro's number, η is solvent viscosity, s is the Svedberg coefficient, ρ is solvent density, r_s is the Stokes radius of the complex, and υ is the partial specific volume of the complex (*19*). A molecular mass of 130210 Da can be calculated from the amino acid composition of recombinant proteins that would make up a heterotetramer composed of two subunits of TarI and two subunits of TarJ.

$$m = \frac{6\pi N_A \eta r_s s}{(1 - \rho\upsilon)} \quad (7)$$

Using the $TarI_2J_2$ model for oligomerization of TarIJ, we turned to sedimentation equilibrium to confirm our findings from sedimentation velocity and gel filtration experiments. Sedimentation equilibrium experiments at concentrations ranging from 4.6 to 9.3 μM were fit best by a model that described dimerization (K_d of 0.76 μM) of a single species corresponding to the mass of a heterooligomer of one subunit of TarI and one subunit of TarJ having a total mass of 65105 Da (Table 1, Supporting Information Figure 3). Thus the oligomerization was found to have a monomer−dimer equilibrium where the association was of stably associated heterodimers (i.e., TarIJ + TarIJ ↔ $TarI_2J_2$).

Steady-State Bisubstrate Kinetic Analysis of Bcs1 and TarIJ Cytidylyltransferase and Reductase Reactions. To address the kinetic mechanisms of the TarIJ and Bcs1 bisubstrate reductase reactions, initial velocity studies were conducted, varying NADPH concentrations at fixed levels of ribulose 5-phosphate. Similarly, a bisubstrate steady-state

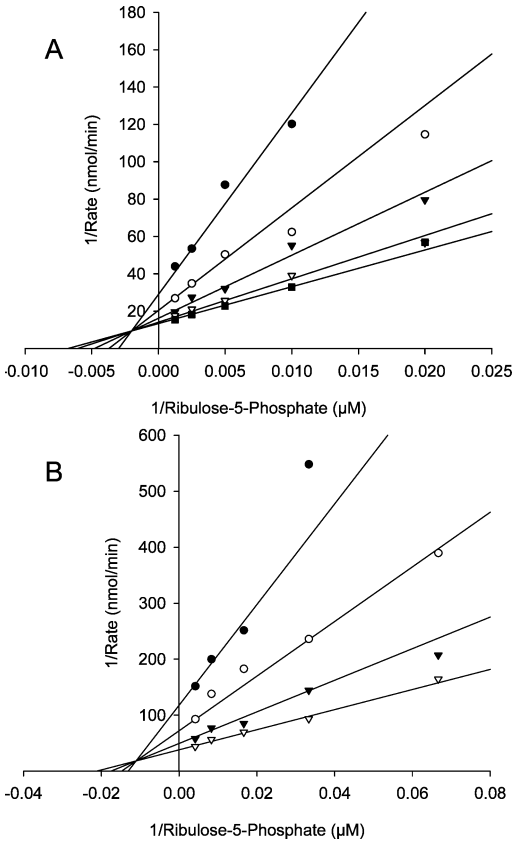

FIGURE 3: Bcs1 and TarIJ initial velocity patterns for the reductase reaction. Initial rate data for the reductase reaction at varying concentrations of NADPH and a fixed concentration of ribulose 5-phosphate. (A) Double reciprocal plots of $1/\upsilon$ versus 1/[S] for Bcs1. The concentration of NADPH was fixed at 5 μM (●), 10 μM (○), 20 μM (▼), 40 μM (▽), and 60 μM (■) while the concentration of ribulose 5-phosphate was varied from 50 to 800 μM. (B) Double reciprocal plots of $1/\upsilon$ versus 1/[S] for TarIJ. The concentration of NADPH was fixed at 2 μM (●), 4 μM (○), 8 μM (▼), and 16 μM (▽) while the concentration of ribulose 5-phosphate was varied between 15 and 240 μM. All data were fit by nonlinear least squares regression to a sequential mechanism where a ternary complex forms, as described by eq 1. Steady-state kinetic parameters can be found in Table 2.

analysis was conducted on the cytidylyltransferase reactions that TarIJ and Bcs1 catalyze by varying CTP at fixed ribitol 5-phosphate concentrations. The intersection of the double reciprocal plots to the left of the y-axis represents the formation of a sequential ternary complex for the reductase reactions (Figure 3) and the cytidylyltransferase reactions (Figure 4) of Bcs1 and TarIJ. The kinetic constants determined for each reaction are outlined in Table 2.

The reductase reactions catalyzed by Bcs1 and by TarIJ show similar Michaelis constants for the reduced cofactor NADPH and the phosphorylated ketose substrate ribulose 5-phosphate; however, they have dissimilar turnover rates. The turnover of Bcs1's reductase reaction is 10-fold higher than that of TarIJ, 7.62 s^{-1} compared to 0.79 s^{-1}. The cytidylyltransferase reactions showed only roughly a 3-fold difference in turnover, 23.5 s^{-1} for Bcs1 and 76.8 s^{-1} for TarIJ; however, they have widely varying Michaelis constants for the reactions. The K_m values for CTP and ribitol 5-phosphate in the case of Bcs1 were 8.51 and 14.7 μM, respectively, compared to 78.9 μM and 1.28 mM for TarIJ, respectively.

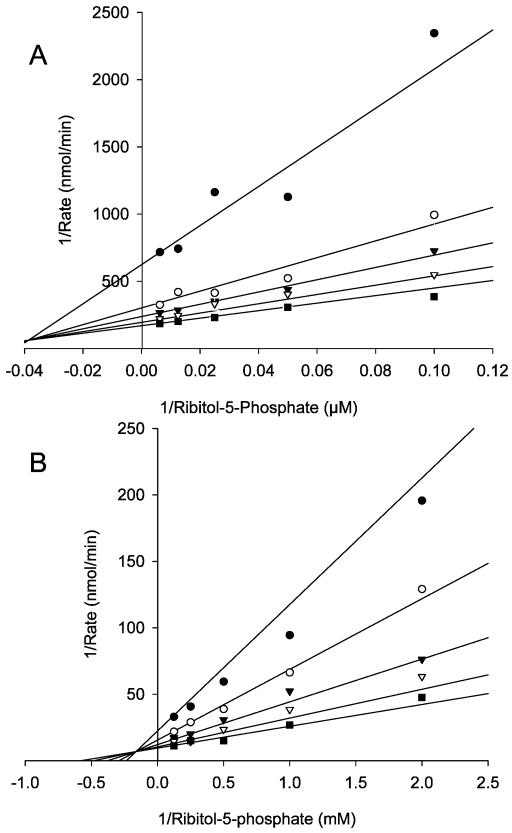

FIGURE 4: Bcs1 and TarIJ initial velocity patterns of the cytidylyltransferase reaction. Initial rate data for the cytidylyltransferase reaction at varying concentrations of CTP and fixed concentrations of ribitol 5-phosphate. (A) Double reciprocal plots of $1/v$ versus 1/[S] for Bcs1. The concentration of CTP was fixed at 2.5 μM (●), 7.5 μM (○), 12.5 μM (▼), 22.5 μM (▽), and 42.5 μM (■) while the concentration of ribitol 5-phosphate was varied from 10 to 80 μM. (B) Double reciprocal plots of $1/v$ versus 1/[S] for TarIJ. The concentration of CTP was fixed at 50 μM (●), 100 μM (○), 200 μM (▼), 400 μM (▽), and 800 μM (■) while the concentration of ribitol 5-phosphate was varied between 0.5 and 8 mM. Reaction progress was monitored by the production of [5-^{3}H]CDP-ribitol using anion-exchange HPLC. All data were fit by nonlinear least squares regression to a sequential mechanism where a ternary complex forms, as described by eq 1. Steady-state parameters are listed in Table 2.

Dissimilar rates and Michaelis constants of the two coupled reactions of TarIJ predict an uneven catalytic turnover between the active sites. In a bifunctional model with intermediate diffusion between the reductase and cytidylyltransferase active sites, the 100-fold difference in rate prevents the accumulation of millimolar concentrations of ribitol 5-phosphate. In most biological systems the intracellular substrate concentration is roughly equivalent to the observed Michaelis constant for an enzyme (*20*, *21*). However, the kinetic constants outlined for TarIJ present a situation where the concentration of the intermediate at steady state will be manyfold lower than the determined K_m of ribitol 5-phosphate for the cytidylyltransferase of TarIJ. Indeed, we have addressed this paradox in some detail in our rapid mixing studies described below.

Product Inhibition Studies on the Bcs1 and TarIJ Reductase Reaction. To discriminate between ordered and random mechanisms and to gain some insight into the order of substrate binding and product release for the reduction of ribulose 5-phosphate to ribitol 5-phosphate, product inhibition studies were performed for TarIJ and Bcs1. In the case of Bcs1, competitive inhibition was observed between NADPH and $NADP^+$ as well as between ribulose 5-phosphate and ribitol 5-phosphate. Noncompetitive/mixed inhibition was observed between the substrate ribulose 5-phosphate and product $NADP^+$ and between the substrate NADPH and product ribitol 5-phosphate (Table 3, Supporting Information Figure 4). A product inhibition pattern comprised of two exclusive competitive substrate−inhibitor pairs suggests a Theorell−Chance mechanism. In this situation of an ordered bi-bi mechanism, product release is rate limiting with essentially no accumulation of the ternary complex. Hence binding order could not be elucidated from product inhibition alone and was supplemented with binding analysis (see below). Nevertheless, the data suggest substrate−product binding pairs composed of the oxidized and reduced cofactors and the two phosphorylated carbohydrates.

Product inhibition of the TarIJ reductase reaction was investigated using the product $NADP^+$ as an inhibitor. Noncompetitive/mixed inhibition was observed between the substrate ribulose 5-phosphate and $NADP^+$ and competitive inhibition between NADPH and $NADP^+$ (Table 3, Supporting Information Figure 5). Using ribitol 5-phosphate as an inhibitor proved to be problematic as no inhibition was observed up to 10 mM. However, from the inhibition patterns observed, an ordered mechanism where NADPH binds first and $NADP^+$ leaves last is implied (Scheme 2). Noncompetitive/mixed inhibition between ribulose 5-phosphate and NADPH excludes a random mechanism, and competitive inhibition between NADPH and $NADP^+$ suggests that these molecules each individually bind to the apo form of the enzyme.

Binding Studies for the Bcs1 Reductase Active Site. To discern binding order for the reductase reaction of Bcs1, the dissociation constants for each substrate were determined. This was necessary as in a Theorell−Chance mechanism only binding pairs can be determined from product inhibition studies. In the case of this mechanism the K_m and K_d for the first binding substrate should be roughly equivalent while the K_m is significantly less than K_d for the second binding substrate (*17*). We used the intrinsic protein fluorescence of Bcs1 to monitor the binding of the substrate ribulose 5-phosphate. The relative change in protein fluorescence on incubation with ribulose 5-phosphate can be fit to a one-site saturation rectangular hyperbola with a K_d of 1.25 mM (Figure 5A). The dissociation constant of NADPH was determined using fluorescence resonance energy transfer (FRET) between active site aromatic amino acids and NADPH. The saturable FRET was fit to a rectangular hyperbola with a K_d of 5.56 μM (Figure 5B). Thus the observed K_m (7.06 μM) and K_d for NADPH are relatively equivalent. For ribulose 5-phosphate, on the other hand, the K_m (106 μM) is 10-fold lower than the K_d for ribulose 5-phosphate. Together, the data suggest that NADPH binds first and that ribulose 5-phosphate binds second (Scheme 2).

Product Inhibition Studies of the Bcs1 and TarIJ Cytidylyltransferase Reaction. Product inhibition studies were conducted on the cytidylyltransferase reactions of Bcs1 and TarIJ. As mentioned earlier, each of these enzymes undergoes ternary complex formation and, hence, requires further studies to elucidate the mechanism. Product inhibition studies

Table 2: Summary of Kinetic Constants

substrate	K_m (μM)	k_{cat} (s^{-1})	K_{ia} (μM)	k_{cat}/K_m (M^{-1}/s^{-1})
reductase				
Bcs1				
NADPH	7.06 ± 1.89	7.41 ± 0.41	33.4 ± 11.2	1.05×10^6
ribulose-5-P	106 ± 24			7.02×10^4
TarIJ				
NADPH	6.74 ± 1.64	0.79 ± 0.06	21.4 ± 11.7	1.17×10^5
ribulose-5-P	28.5 ± 13.1			2.77×10^4
cytidylyltransferase				
Bcs1				
CTP	8.51 ± 1.50	23.5 ± 1.42	15.0 ± 6.1	2.76×10^6
ribitol-5-P	14.7 ± 3.5			1.59×10^6
TarIJ				
CTP	78.9 ± 33.2	76.8 ± 6.5	376 ± 168	9.73×10^5
ribitol-5-P	1280 ± 390			5.98×10^4

Table 3: Summary of Reductase Product Inhibition Studies

inhibitor	varied substrate	fixed substrate	pattern of inhibition	K_{ii} (μM)[a]	K_{is} (μM)[b]
Bcs1[c]					
$NADP^+$	NADPH	ribulose-5-P (200 μM)	competitive		173 ± 26
$NADP^+$	ribulose-5-P	NADPH (20 μM)	noncompetitive/mixed	430 ± 24	
ribitol-5-P	NADPH	ribulose-5-P (200 μM)	noncompetitive/mixed	140 ± 7.1	
ribitol-5-P	ribulose-5-P	NADPH (20 μM)	competitive		46.1 ± 6.6
TarIJ[d]					
$NADP^+$	NADPH	ribulose-5-P (60 μM)	competitive		96.8 ± 16.2
$NADP^+$	ribulose-5-P	NADPH (10 μM)	noncompetitive/mixed	310 ± 130	403 ± 101
ribitol-5-P	NADPH	ribulose-5-P (60 μM)			>10 mM
ribitol-5-P	ribulose-5-P	NADPH (10 μM)			>10 mM

[a] K_{ii}, $K_{i(intercept)} = \alpha K_i$. [b] K_{is}, $K_{i(slope)} = K_i$. [c] Data derived from nonlinear regression. See Supporting Information Figure 4. [d] Data derived from nonlinear regression. See Supporting Information Figure 5.

of the cytidylyltransferase activity of Bcs1 demonstrated competitive inhibition between the phosphorylated carbohydrate ribitol 5-phosphate and inorganic pyrophosphate. However, noncompetitive/mixed inhibition was observed among all other substrate−product pairs (Table 4, Supporting Information Figure 6). Product inhibition patterns with a single competitive substrate−inhibitor pairing are indicative of an ordered bi-bi mechanism. Additionally, the competitive pairing designates the first binding substrate, ribitol 5-phosphate, and the last product to leave the active site, pyrophosphate. To test the competitive nature of inorganic pyrophosphate with the substrate ribitol 5-phosphate, the latter was held at saturating concentrations while CTP and pyrophosphate were varied. No inhibition was observed as the high substrate concentration out-competed inhibition from the product. This is consistent with an ordered bi-bi mechanism, as saturating concentrations of the first binding substrate should negate any inhibition from its competitive partner.

Product inhibition studies on the cytidylyltransferase reaction of the TarIJ complex revealed competitive inhibition between the CDP-ribitol product and the substrate CTP. Noncompetitive/mixed inhibition was observed among all other substrate−product pairs (Table 4, Supporting Information Figure 7). The pattern of product inhibition suggests an ordered bi-bi mechanism with the substrate CTP binding first and the product CDP-ribitol leaving last. An additional test with saturating concentrations of CTP while varying ribitol 5-phosphate and CDP-ribitol concentrations revealed no inhibition from the product. Competition of the substrate with the inhibitor CDP-ribitol confirmed the ordered bi-bi mechanism with CTP binding first and CDP-ribitol leaving last. The kinetic mechanism of the cytidylyltransferase reaction that the TarIJ complex catalyzes is similar to that of Bcs1 in that it is ordered; however, the order of substrate binding and product release are dissimilar and, in fact, are inverted (Scheme 3). That is, the substrates have interchanged the order of primary binding as well as the order of product release.

Rapid Mixing Experiments and Steady-State Reaction Modeling for TarIJ. To examine the possibility of substrate channeling between the two enzymes in the TarIJ complex, we used rapid mixing methodology to examine the lag time to approach steady-state as well as steady-state intermediate concentration. Starting with CTP, ribulose 5-phosphate, and NADPH and monitoring both the reductase (stopped flow) and cytidylyltransferase (rapid quench) reactions, we observed a significant lag (~300 s) to reach steady state, corresponding to the time required to accumulate approximately a 12 μM amount of the intermediate ribitol 5-phosphate (Figure 6). Modeling of the reaction with the steady-state parameters outlined in Table 2 suitably predicted the time course for depletion of substrates and production of intermediate and of products (Figure 6). The fact that the time course for the bifunctional reaction was consistent with that predicted by steady-state kinetic parameters for each active site suggested that the intermediate ribitol 5-phosphate was not channeled between active sites but released to the bulk solvent. The high ribitol 5-phosphate K_m and high cytidylyltransferase turnover, relative to the reductase turnover to which it is coupled, create a situation where the cytidylyltransferase active site operates at a substrate concentration 100-fold lower than its K_m.

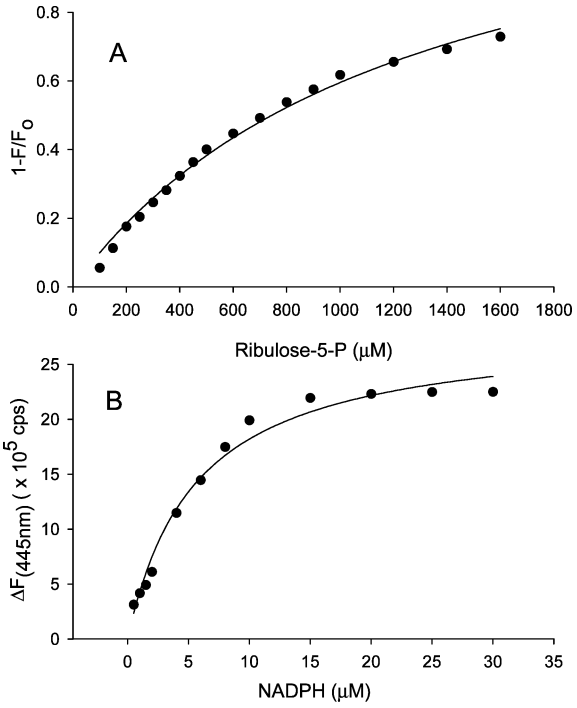

FIGURE 5: Determination of dissociation constants of NADPH and ribulose 5-phosphate for the Bcs1 protein. (A) Excitation of Bcs1 at 284 nm resulted in fluorescence resonance energy transfer (FRET) to bound NADPH with an emission maximum of 445 nm. Shown is the FRET as a function of NADPH added. Fit of the data to a rectangular hyperbola yielded a dissociation constant of 5.56 ± 0.52 μM for NADPH. (B) Intrinsic protein fluorescence quenching of 1 μM Bcs1 was observed upon addition of substrate ribulose 5-phosphate (1−1600 μM). Protein fluorescence spectra were monitored between 300 and 360 nm after excitation at 284 nm. The relative change in fluorescence upon regression to a rectangular hyperbola resulted in a dissociation constant of 1.25 ± 0.10 mM. Fluorescence spectra were collected using a PTI spectrofluorometer (Photon Technologies International, London, Ontario, Canada). The mixture was composed of 25 mM HEPES, 1 mM DTT, 85 μM CTP, 10 mM $MgCl_2$, and 0.01 mg/mL BSA degassed through vacuum filtration and bubbled with nitrogen gas to displace dissolved oxygen. Control spectra of buffer alone, protein and buffer, and substrate and buffer were used to correct for changes in fluorescence not due to protein−ligand binding. FRET and intrinsic protein fluorescence quenching data were fit to a rectangular hyperbola using the Enzyme Kinetics Module v1.1 of Sigmaplot 8.0.

Scheme 2: Theorell−Chance Mechanism Proposed for the Reductase Reaction of Bcs1 (Top) and Ordered Bi−Bi Mechanism Proposed for the Reductase Reaction of TarIJ (Bottom)

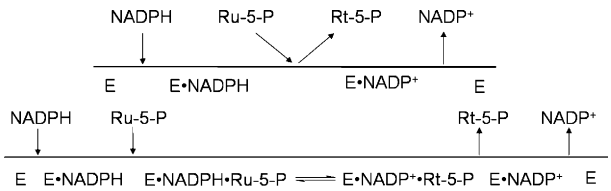

DISCUSSION

The evolutionary logic of fusion and/or complex formation of protein modules to create multifunctional proteins has been the subject of curious study by enzymologists for many years. It has been argued that heterooligomerization increases the effective concentrations of, for example, enzymes in a metabolic pathway, easing the limitations of small molecule diffusion within complex organisms or preventing side reactions occurring with intermediates that produce toxic effects (*22*, *23*). More recently, the question of gene fusion has also been a focal point for a whole-genome computational approach referred to as the Rosetta stone theory for gene annotation. The thesis that fusion to form a composite protein encoded in the genome of one organism often implies functional association of separate component proteins in another has proven effective in functional annotation of genes of unknown function (*12*−*14*).

From the composite protein Bcs1 from *H. influenzae*, we predicted a functional association and physical interaction between the proteins TarI and TarJ using the Rosetta stone criteria. The prediction was that TarI and TarJ would functionally associate to form CDP-ribitol synthase in *S. aureus*. Interestingly, orthologous domains were found solely in cytidylyltransferase domains (N-terminal region of Bcs1 and TarI) while reductase domains were analogous (C-terminus of Bcs1 and TarJ). Thus while the Rosetta stone criteria were not strictly upheld, TarI and TarJ proved to associate to form an active CDP-ribitol synthase complex. In this work we present data outlining the kinetic mechanisms of the cytidylyltransferase and reductase reactions along with biophysical data pertaining to the oligomeric state of the CDP-ribitol synthases from *H. influenzae* and *S. aureus*.

Hydrodynamic experiments presented here demonstrated that both Bcs1 and TarIJ form higher order oligomers. A monomer−dimer equilibrium (K_d of 1.3 μM) was evident for Bcs1 with the dimer predominating in the presence of substrate CTP and $MgCl_2$. The oligomerization of TarIJ was best described by a model where a TarIJ heterodimer could undergo homodimerization (K_d of 0.8 μM) to form a complex corresponding to two subunits of TarI and two subunits of TarJ ($TarI_2J_2$). The presence of higher order oligomers may suggest allosteric regulation of CDP-ribitol synthase activity through heterotrophic effector molecules (*24*). Indeed, stabilization of the reductase activity of Bcs1 with CTP and $MgCl_2$ (*6*) of the dimeric structure observed here may indicate some level of biochemical regulation by substrates.

Initial velocity bisubstrate analysis, product inhibition experiments, and fluorescence binding studies revealed kinetic mechanisms for the reductase and cytidylyltransferase reactions of Bcs1 and TarIJ. We found that the reductase reaction of Bcs1 followed a Theorell−Chance mechanism (*17*), a special case of ordered bi-bi mechanism with very little accumulation of a ternary complex. NADPH binds first and $NADP^+$ is the final departing product for Bcs1. In the case of the reductase reaction of TarIJ, product inhibition experiments could not be completed, but the data were most consistent with an ordered mechanism identical to that proposed for Bcs1. Such a mechanism is common for members of the zinc-dependent alcohol dehydrogenase family (*25*).

Steady-state kinetic studies were additionally used to probe the mechanism of cytidylyltransferase by Bcs1 and TarIJ. It was found that these activities were ordered with identical substrate−product binding pairs; however, the order of binding was inverted. The reaction of Bcs1 followed a kinetic mechanism where ribitol 5-phosphate binding is followed by CTP. After nucleotidyl transfer, CDP-ribitol is the first product to leave followed by pyrophosphate. This mechanism

Table 4: Summary of Cytidylyltransferase Product Inhibition Studies

inhibitor	varied substrate	fixed substrate	pattern of inhibition	K_{ii} (μM)[a]	K_{is} (μM)[b]
Bcs1[c]					
CDP-ribitol	ribitol-5-P	CTP (20 μM)	noncompetitive/mixed	40.8 ± 2.5	
CDP-ribitol	CTP	ribitol-5-P (40 μM)	noncompetitive/mixed	114 ± 56	19.7 ± 3.5
PP_i	ribitol-5-P	CTP (20 μM)	competitive		9.40 ± 1.42
PP_i	CTP	ribitol-5-P (40 μM)	noncompetitive/mixed	48.0 ± 5.6	
PP_i	CTP	ribitol-5-P (1 mM)	no inhibition		
TarIJ[d]					
CDP-ribitol	ribitol-5-P	CTP (200 μM)	noncompetitive/mixed	420 ± 30	
CDP-ribitol	CTP	ribitol-5-P (2000 μM)	competitive		340 ± 50
PP_i	ribitol-5-P	CTP (200 μM)	noncompetitive/mixed	2040 ± 210	
PP_i	CTP	ribitol-5-P (2000 μM)	noncompetitive/mixed	1390 ± 170	
CDP-ribitol	ribitol-5-P	CTP (7.5 mM)	no inhibition		

[a] K_{ii}, $K_{i(intercept)} = \alpha K_i$. [b] K_{is}, $K_{i(slope)} = K_i$. [c] Data derived from nonlinear regression. See Supporting Information Figure 6. [d] Data derived from nonlinear regression. See Supporting Information Figure 7.

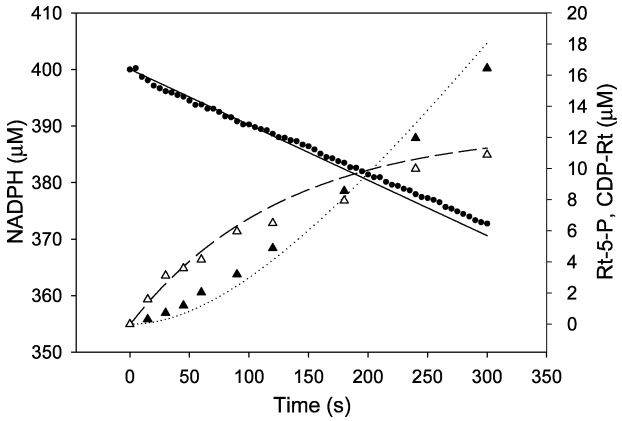

FIGURE 6: Bifunctional catalysis of the TarIJ−enzyme complex following rapid mixing of 125 nM enzyme with a saturating concentration of ribulose 5-phosphate (400 μM), CTP (400 μM, 0.25 Ci/mmol), and NADPH (400 μM). Shown are the time course of NADPH depletion (●), CDP-ribitol formation (▲), and the calculated concentration of the intermediate ribitol 5-phosphate (△). The reductase reaction was monitored through the observation in a decrease of absorbance at 340 nm using a stopped-flow apparatus over a course of six trials. The cytidylyltransferase reaction was monitored by rapid quench through the conversion of [5-^{3}H]CTP to [5-^{3}H]CDP-ribitol using anion-exchange HPLC with in-line radioactivity detection performed in duplicate. The concentration of the intermediate ribitol 5-phosphate was calculated from the difference between the reductase turnover and the product CDP-ribitol concentrations. Modeled data were calculated through numerical integration at 1 s intervals using steady-state parameters listed in Table 2. The solid, dashed, and dotted lines represent the theoretical concentrations of the substrate NADPH, reaction intermediate D-ribitol 5-phosphate, and product CDP-ribitol, respectively, using the steady-state kinetic parameters for TarIJ described in this work. The concentration of NADPH at any given time t was equal to 400 μM $- \sum^t k_{cat}$[E][NADPH]$_t$/(K_m + [NADPH]$_t$), where $k_{cat} = 0.8$ s^{-1}, $K_m = 6.74$ μM, and [E] = 0.125 μM. The concentration of CDP-ribitol at any given time t was equal to $\sum^{t-1} k_{cat}$[E][Rt-5-P]$_{t-1}$/(K_m + [Rt-5-P]$_{t-1}$), where $k_{cat} = 78.9$ s^{-1}, $K_m = 1283$ μM, and [E] = 0.125 μM. The concentration of ribitol 5-phosphate was equal to the difference between the decrease in NADPH and the concentration of CDP-ribitol at time t. The reaction components consisted of 25 mM HEPES, pH 7.2, 0.4 mM CTP, 0.4 mM ribulose 5-phosphate, 0.4 mM NADPH, 10 mM $MgCl_2$, 0.01% Triton X-100, 5 μCi of [5-^{3}H]CTP, and 125 nM TarIJ. Rapid mixing experiments were performed on the TarIJ bifunctional complex using a SFM-400/S mixer with a MOS-250 optical unit (Molecular Kinetics, Pullman, WA).

is similar to that determined for the TarD enzyme that catalyzes the formation of a teichoic acid linkage unit precursor CDP-glycerol in *S. aureus* from glycerol 3-phosphate and CTP (*16*). In contrast, experiments reported here with TarIJ indicated that CTP binds first, followed by ribitol 5-phosphate. Postcatalysis, the product pyrophosphate exits the active site, followed by the activated precursor CDP-ribitol. The difference in kinetic mechanism seen with the two cytidylyltransferases was surprising given the extensive sequence similarity between TarI and the N-terminal domain of Bcs1. While little mechanistic information exists for related bacterial nucleotidyltransferases, our findings are interesting in light of crystal structural information on the homologues 4-diphosphocytidyl-2-*C*-methylerythritol synthetase (IspD/YgbP) and *N*-acetylglucosamine-1-phosphate uridylyltransferase (GlmU). In the case of the former, costructures with substrates bound are most consistent with a sequential mechanism where the nucleotide binds first and the nucleotide diphosphosugar derivative exits last (*9*). Structural analysis of GlmU, on the other hand, reveals a large open active site (*8*, *26*) that potentially could accommodate either mechanism.

Scheme 3: Ordered Bi-Bi Mechanisms Proposed for the Cytidylyltransferase Reactions of Bcs1 (Top) and TarIJ (Bottom)

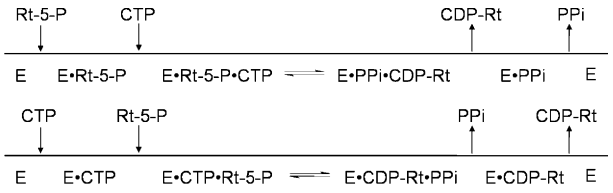

Having previously determined that Bcs1 catalyzed bifunctional turnover in distinct active sites with the release and free diffusion of the metabolic intermediate ribitol 5-phosphate (*6*), we were reluctant to consider the possibility of intermediate channeling by TarIJ. Nevertheless, our steady-state kinetic analysis raised some doubt as substrate binding order appeared to be different in TarIJ. Furthermore, in the case of TarIJ, the intermediate ribitol 5-phosphate had a high K_i (>10 mM) for the reductase and high K_m (1.28 mM) for the cytidylyltransferase reaction. The high K_m (and K_i) value for the intermediate suggested that it might be maintained at a high concentration in a channel between the active sites. The 100-fold difference in k_{cat} between the two functions in TarIJ was likewise remarkable and not shared with Bcs1. These differences led us to consider the plausibility of substrate channeling in TarIJ and to investigate this idea using rapid mixing methods.

Substrate channeling is thought to be advantageous where the intermediate is chemically liable, reacts with a diffusion-controlled limit, or is cross-reactive with other enzymatic reactions (*27*−*30*). The metabolite ribitol 5-phosphate is not especially labile, nor does it undergo cytidylyl transfer in TarIJ at a diffusion-controlled limit (k_{cat}/K_m, 5.98×10^4 M^{-1} s^{-1}). Rapid mixing experiments were used here to follow the approach to steady-state catalysis in the bifunctional reaction by following the formation of products $NADP^+$ and CDP-ribitol on incubation with substrates NADPH, ribulose 5-phosphate, and CTP. These experiments indicated a rapid oxidation of NADPH with a significant lag in the approach to steady-state cytidylyl transfer. The lag was entirely consistent with the accumulation of a sub-K_m concentration (12 μM) of ribitol 5-phosphate predicted by the steady-state kinetic constants, indicating that catalysis by TarIJ occurs with release and free diffusion of the metabolic intermediate ribitol 5-phosphate. Therefore, while channeling appears not to limit the release of ribitol 5-phosphate by TarIJ, the 100-fold difference in k_{cat} observed between the reductase and cytidylyltransferase activities creates a situation where the accumulation of K_m concentrations of ribitol 5-phosphate is prevented. Typically, enzymes have K_m values that correspond to intracellular substrate concentrations (*20*, *21*). It is conceivable that the relatively low concentration of ribitol 5-phosphate accumulated relative to K_m for TarIJ reflects a need in *S. aureus* to limit the concentration of this metabolite to curtail competing, undesirable side reactions. It is interesting to note that, in the case of TarIJ, the preferred binding order for the cytidylyltransferase reaction has CTP binding to the apo form of the enzyme, priming it for collision with freely diffusing molecules of ribitol 5-phosphate.

Bifunctional enzymes are thought to be distinctive and highly conserved products of relatively infrequent gene fusion events that link two proteins of separate yet related functions (*12*, *13*). The Rosetta stone hypothesis thus argues functional and physical association among individual component proteins that show orthology to distinct domains of multifunctional composite enzymes. This argument therefore relies on evolutionary relationships between the component and composite proteins. It is intriguing to note from our work here that while the reductase TarJ shows a nonevolutionary (analogous) relationship with the reductase domain of Bcs1, the predictions of the Rosetta stone theory still hold. Hence, we have documented in this work a remarkable functional and physical association of TarI and TarJ to form an active CDP-ribitol synthase.

Here we report experiments aimed at understanding the structure and mechanism of the bifunctional CDP-ribitol synthases, Bcs1 and TarIJ, key enzymes in the synthesis of virulence-associated polyol phosphates in *H. influenzae* and *S. aureus*, respectively. Our work highlights an unusual Rosetta stone relationship between Bcs1 and TarIJ and provides a mechanistic foundation for understanding the association of reductase and cytidylyltransferase activities in these bifunctional proteins. These and ongoing studies will help to define strategies for the development of novel antimicrobials that prevent the synthesis of activated precursors to virulence-associated polysaccharides.

ACKNOWLEDGMENT

We thank David Badurina for the creation of the overexpression vector pDest14-TarIJ.

SUPPORTING INFORMATION AVAILABLE

Product inhibition plots for both the reductase and cytidylyltransferase reactions and sedimentation equilibrium and sedimentation velocity data for Bcs1 and TarIJ. This material is available free of charge via the Internet at http://pubs.acs.org.

REFERENCES

1. Branefors-Helander, P. (1977) The structure of the capsular antigen from *Haemophilus influenzae* type A, *Carbohydr. Res. 56*, 117−122.
2. Weidenmaier, C., Kokai-Kun, J. F., Kristian, S. A., Chanturiya, T., Kalbacher, H., Gross, M., Nicholson, G., Neumeister, B., Mond, J. J., and Peschel, A. (2004) Role of teichoic acids in *Staphylococcus aureus* nasal colonization, a major risk factor in nosocomial infections, *Nat. Med. 10*, 243−245.
3. Crisel, R. M., Baker, R. S., and Dorman, D. E. (1975) Capsular polymer of *Haemophilus influenzae*, type b. I. Structural characterization of the capsular polymer of strain Eagan, *J. Biol. Chem. 250*, 4926−4930.
4. Kojima, N., Araki, Y., and Ito, E. (1983) Structure of linkage region between ribitol teichoic acid and peptidoglycan in cell walls of *Staphylococcus aureus* H, *J. Biol. Chem. 258*, 9043−9045.
5. Kaya, S., Yokoyama, K., Araki, Y., and Ito, E. (1984) *N*-acetylmannosaminyl(1→4)*N*-acetylglucosamine, a linkage unit between glycerol teichoic acid and peptidoglycan in cell walls of several *Bacillus* strains, *J. Bacteriol. 158*, 990−996.
6. Zolli, M., Kobrick, D. J., and Brown, E. D. (2001) Reduction precedes cytidylyltransfer without substrate channeling in distinc active sites of the bifunctional CDP-ribitol synthase from *Haemophilus influenzae*, *Biochemistry 40*, 5041−5048.
7. Mio, T., Yabe, T., Arisawa, M., and Yamada-Okabe, H. (1998) The eukaryotic UDP-*N*-acetylglucosamine pyrophosphorylases. Gene cloning, protein expression, and catalytic mechanism, *J. Biol. Chem. 273*, 14392−14397.
8. Olsen, L. R., and Roderick, S. L. (2001) Structure of the *Escherichia coli* GlmU pyrophosphorylase and acetyltransferase active sites, *Biochemistry 40*, 1913−1921.
9. Richard, S. B., Bowman, M. E., Kwiatkowski, W., Kang, I., Chow, C., Lillo, A. M., Cane, D. E., and Noel, J. P. (2001) Structure of 4-diphosphocytidyl-2-C-methylerythritol synthetase involved in mevalonate-independent isoprenoid biosynthesis, *Nat. Struct. Biol. 8*, 641−648.
10. Jornvall, H., Persson, B., Krook, M., Atrian, S., Gonzalez-Duarte, R., Jeffery, J., and Ghosh, D. (1995) Short-chain dehydrogenases/reductases (SDR), *Biochemistry 34*, 6003−6013.
11. Jornvall, H., Persson, B., and Jeffery, J. (1987) Characteristics of alcohol/polyol dehydrogenases. The zinc-containing long-chain alcohol dehydrogenases, *Eur. J. Biochem. 167*, 195−201.
12. Marcotte, E. M., Pellegrini, M., Ng, H. L., Rice, D. W., Yeates, T. O., and Eisenberg, D. (1999) Detecting protein function and protein−protein interactions from genome sequences, *Science 285*, 751−753.
13. Enright, A. J., Iliopoulos, I., Kyrpides, N. C., and Ouzounis, C. A. (1999) Protein interaction maps for complete genomes based on gene fusion events, *Nature 402*, 86−90.
14. Yanai, I., Derti, A., and DeLisi, C. (2001) Genes linked by fusion events are generally of the same functional category: a systematic analysis of 30 microbial genomes, *Proc. Natl. Acad. Sci. U.S.A. 98*, 7940−7945.
15. Gill, S. C., and von Hippel, P. H. (1989) Calculation of protein extinction coefficients from amino acid sequence data, *Anal. Biochem 182*, 319−326.
16. Badurina, D. S., Zolli-Juran, M., and Brown, E. D. (2003) CTP: glycerol 3-phosphate cytidylyltransferase (TarD) from *Staphylococcus aureus* catalyzes the cytidylyl transfer via an ordered Bi−Bi reaction mechanism with micromolar K(m) values, *Biochim. Biophys. Acta 1646*, 196−206.
17. Segel, I. H. (1975) *Enzyme kinetics: behavior and analysis of rapid equilibrium and steady-state enzyme systems*, Wiley, New York.

18. McRorie, D. K., and Voelker, P. J. (1993) *Self-Associating Systems in the Analytical Ultracentrifuge*, Beckman Instruments, Fullerton, CA.
19. Siegel, L. M., and Monty, K. J. (1966) Determination of molecular weights and frictional ratios of proteins in impure systems by use of gel filtration and density gradient centrifugation. Application to crude preparations of sulfite and hydroxylamine reductases, *Biochim. Biophys. Acta 112*, 346−362.
20. Atkinson, D. E. (1969) in *Current Topics in Cellular Regulation* (Horecker, B. L., and Stadtman, E. R., Eds.) pp 29−43, Academic Press, New York.
21. Cornish-Bowden, A. (1976) The effect of natural selection on enzymic catalysis, *J. Mol. Biol. 101*, 1−9.
22. Liang, P. H., and Anderson, K. S. (1998) Substrate channeling and domain-domain interactions in bifunctional thymidylate synthase-dihydrofolate reductase, *Biochemistry 37*, 12195−12205.
23. Ovadi, J. (1991) Physiological significance of metabolic channelling, *J. Theor. Biol. 152*, 1−22.
24. Helmstaedt, K., Krappmann, S., and Braus, G. H. (2001) Allosteric regulation of catalytic activity: *Escherichia coli* aspartate transcarbamoylase versus yeast chorismate mutase, *Microbiol. Mol. Biol. Rev. 65*, 404−421.
25. Wratten, C. C., and Cleland, W. W. (1963) Product inhibition studies on yeast and liver alcohol dehydrogenases, *Biochemistry 338*, 935−941.
26. Brown, K., Pompeo, F., Dixon, S., Mengin-Lecreulx, D., Cambillau, C., and Bourne, Y. (1999) Crystal structure of the bifunctional *N*-acetylglucosamine 1-phosphate uridyltransferase from *Escherichia coli*: a paradigm for the related pyrophosphorylase superfamily, *EMBO J. 18*, 4096−4107.
27. Srere, P. A. (1987) Complexes of sequential metabolic enzymes, *Annu. Rev. Biochem. 56*, 89−124.
28. Anderson, K. S. (1999) Fundamental mechanisms of substrate channeling, *Methods Enzymol. 308*, 111−145.
29. Welch, G. R., and Easterby, J. S. (1994) Metabolic channeling versus free diffusion: transition-time analysis, *Trends Biochem. Sci. 19*, 193−197.
30. Miles, E. W., Rhee, S., and Davies, D. R. (1999) The molecular basis of substrate channeling, *J. Biol. Chem. 274*, 12193−12196.
31. Laemmli, U. K. (1970) Cleavage of structural proteins during the assembly of the head of bacteriophage T4, *Nature 227*, 680−685.

BI048866V